Rigid body motion tracking in Axial Shift Mapping for measuring astronomical X-ray mirror figure

Brandon D. Chalifoux[a,*], Hayden J. Wisniewski[a],
Mark L. Schattenburg[b], Ralf K. Heilmann[b],
Ian J. Arnold[a], Mallory M. Whalen[c]

[a] James C. Wyant College of Optical Sciences, University of Arizona, Tucson AZ, USA
[b] Kavli Institute for Astrophysics and Space Research, Massachusetts Institute of Technology, Cambridge MA, USA
[c] Department of Mechanical Engineering, Massachusetts Institute of Technology, Cambridge MA, USA
*bchal@arizona.edu

ABSTRACT

Future X-ray telescopes will require measuring thousands of grazing-incidence mirrors with nanometer accuracy and high throughput. Fizeau interferometry will require accurately separating the reference surface from the surface under test, a challenging proposition for optical surfaces that are highly off-axis conics. We present a lateral shifting interferometry approach called Axial Shift Mapping (ASM), in which we measure the surface under test at multiple positions and numerically separate the reference and test surfaces. In this paper, we estimate the measurement accuracy that would be required for an exemplary 0.5 arcsecond half-power diameter angular resolution telescope. We mathematically describe the procedure for using ASM, plus a lateral shift, to extract the most important quantities for X-ray telescope mirrors: axial profile (including the quadratic component) and cone angle variation. We also conclude that the radius and cone angle of a mirror are unknowable with ASM alone.

Keywords: interferometry, X-ray optics, manufacturing, off-axis conics, self-referencing metrology

1. INTRODUCTION

High resolution and high throughput X-ray telescopes, such as the one envisioned in the Lynx X-ray Observatory concept, would enable astronomers to study the evolution of black holes, gas flows in the Cosmic Web, and energetic processes in stellar systems, with orders of magnitude higher sensitivity and resolution than previously attainable [1]. In support of the scientific objectives of *Lynx*, the National Academy of Sciences' 2020 Astrophysics Decadal Survey recommended a potential X-ray probe mission, followed by a future X-ray Great Observatory [2]. Probe concepts like AXIS [3] and HEX-P [4] each call for thin (< 1 mm thick), high resolution grazing incidence X-ray optics. Building sufficiently thin yet accurate grazing incidence X-ray optics represents one of the most significant challenges to realizing a telescope with sub-arcsecond angular resolution (half-power diameter, HPD) and square meters of effective area at ~1 keV X-ray energy. Accurate metrology of these optics remains a challenge.

The optical surfaces are highly off-axis conic sections and must have figure accuracy of only a few nanometers root mean-square (RMS). Due to grazing incidence reflection angles around 1° required for efficient broadband reflection of X-rays, around 150 square meters of mirror area must be produced per square meter of effective area, thus requiring high throughput metrology to enable multiple measurement cycles per mirror. In this sense, a 2 m^2 effective area X-ray telescope requires producing and measuring mirror area and accuracy on par with the Extremely Large Telescopes (ELTs) [5–7] currently under development. As with the ELTs, interferometry is the most mature metrology technique for future X-ray telescopes.

Due to the highly off-axis conic shape of grazing-incidence X-ray optics, null testing requires a nearly cylindrical null corrector to transform a planar wavefront from a Fizeau interferometer to match the X-ray mirror shape (Fig. 1). The measurement of a Fizeau interferometer represents the difference between a wavefront reflected off the reference surface, and a wavefront reflected off the surface under test (SUT) and transmitted through the null corrector optics. The largest contributor to measurement uncertainty of the SUT is generally the uncertainty of the wavefront deformation from the reference surface and the null optics (here, together these are called the reference). We recently introduced Axial Shift Mapping (ASM) [8], a self-referencing interferometry technique for near-cylindrical mirrors wherein the SUT is translated with respect to the reference between measurements. The intended use of ASM is to characterize SUTs or null correctors that can be used as reference optics for manufacturing X-ray optics.

Optics and Photonics for Advanced Dimensional Metrology III, edited by Peter J. de Groot, Felipe Guzman, Pascal Picart, Proc. of SPIE Vol. 12997, 129970U ·
 · 0277-786X · doi: 10.1117/12.3025087

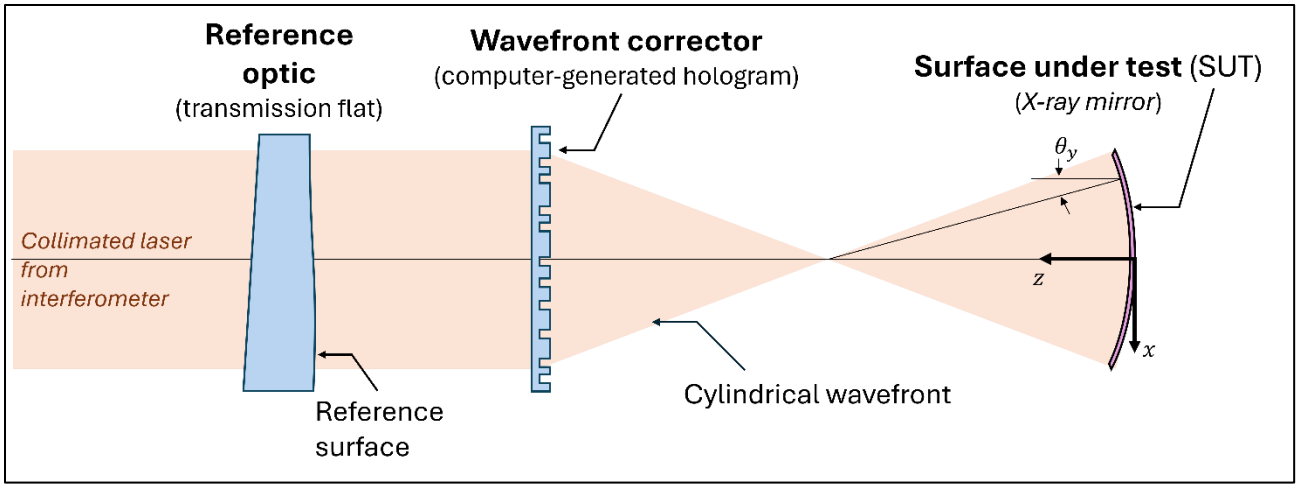

Figure 1. A typical Fizeau interferometry setup. A reference optic (here, a transmission flat) partially reflects a wavefront from the interferometer instrument. The transmitted portion of the wavefront propagates through a wavefront corrector (here, a computer-generated hologram), off the surface under test (here, a near-cylindrical X-ray mirror), then back into the interferometer. The two wavefronts interfere on a detector, from which their phase difference can be determined.

We have previously shown that if two rigid body rotations ($e_{\theta x}$ and $e_{\theta z}$, which are rotations about the x- and z-axis, respectively, in the coordinate frame shown in Fig. 1) are accurately measured during the translation motion in ASM, then the SUT and reference can be unambiguously separated from one another, significantly reducing the systematic measurement uncertainty of the SUT. In our previous work, we only shifted in one direction, along the axis of the cylinder (y-direction in Fig. 1). This enabled unambiguous measurement of the profile along each axial trace of the mirror, denoted here as a line under test (LUT). However, ASM did not enable the tilt of each LUT, with respect to the cylinder axis, to be determined. For X-ray optics (Fig. 2), this results in uncertainty in the local cone angle error of the mirror, which significantly impacts imaging performance of the telescope. In this paper, we show mathematically that the local cone angle error of the mirror can be determined using two ASM sequences each with the SUT at separate lateral positions (i.e., rotated about the cylinder axis). This does not require tracking any additional rigid body motions.

In Section 2, we review the basic metrology requirements of X-ray mirrors. Section 3 details the ASM concept of operation and the extraction process for all relevant X-ray mirror surface figure terms. Section 4 identifies areas of future work and summarizes the presented material.

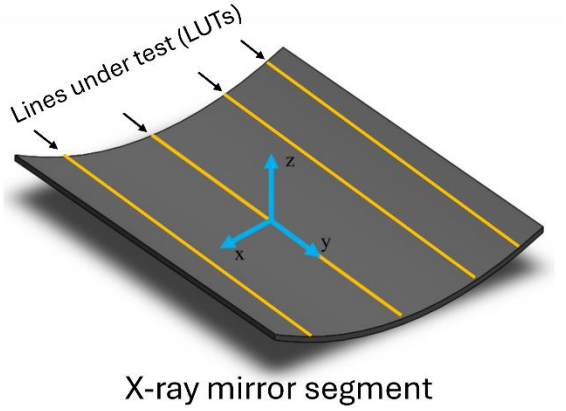

Figure 2. An X-ray mirror segment. The axial profiles are measured along the LUTs as shown in yellow. The telescope optical axis is nearly parallel to the y-axis as shown, and X-rays reflect at grazing incidence off the mirror approximately along that direction.

2. METROLOGY REQUIREMENTS FOR SUB-ARCSECOND RESOLUTION X-RAY OPTICS

Grazing incidence X-ray astronomical telescope optics typically comprise a primary and secondary mirror, each with an axial profile following a Wolter Type I [9] or Wolter-Schwarzschild [10] prescription (Fig. 2). These prescriptions typically exhibit only a few μm departure from a cone, with half-cone angle α_p and $\alpha_s = 3\alpha_p$ for the primary and secondary mirrors, respectively. The radius of a mirror shell is defined at the intersection of the primary and secondary mirror segments, $r_0 = f \sin 4\alpha_p$, where f is the telescope focal length. In some cases—such as with meta-shell optics [11] or adjustable optics [12]—the X-ray mirror shells are segmented into parts each with a small angular span, whereas in other cases [13] the mirror shells are monolithic. Since the angular span of an interferometer is limited, it is only feasible to measure one segment of an X-ray mirror shell at a time, regardless of whether the shell itself is segmented. For simplicity, we will assume the shell is segmented.

Since ASM requires shifting a mirror generally along the axial direction of the cone, we compare a representative mirror segment to a cylindrical surface. Figure 3 shows the difference between a cylinder and a segment of a secondary mirror shell (called the cylindrical departure) with $f = 10\ m$, $r_0 = 0.25\ m$ and a 18° azimuthal span of the segment. The axis of the cylinder is tilted by α_s with respect to the telescope optical axis. The slopes of the cylindrical departure along the axial and azimuthal directions are also shown. The azimuthal slopes represent up to 4 interference fringes per mm, which may result in even denser fringes on the interferometer camera due to anamorphic magnification of the null corrector. In practice, these large slopes may require a null corrector that generates a non-cylindrical wavefront. This is beyond the scope of the current work.

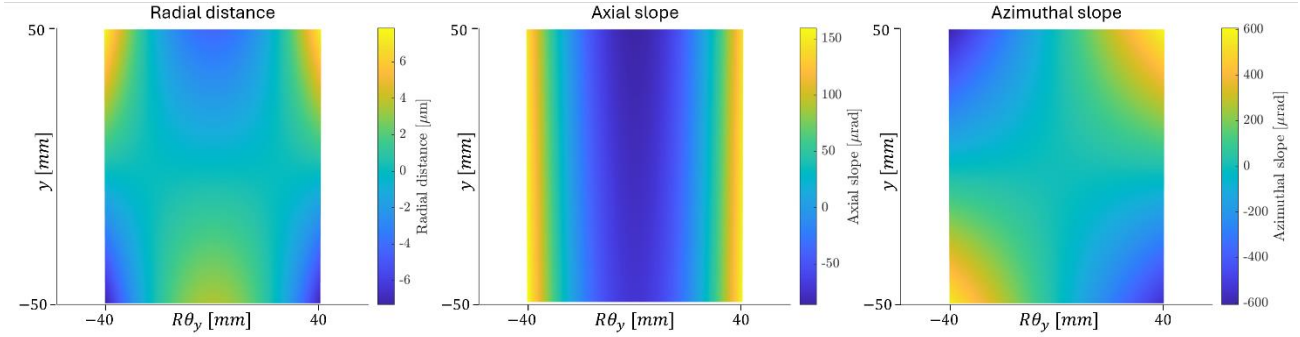

Figure 3. Cylindrical departure of an exemplary X-ray telescope mirror with radius (at the intersection between primary and secondary mirrors) of 250 mm, and a focal length of 10 m. This mirror is the secondary mirror, with a cone angle of 1.07°.

The angular resolution of an X-ray telescope is primarily governed by the axial slope errors of the mirrors. The angular ray deviation produced by a local axial slope error of a mirror, β_{ax}, is $\gamma_{ax} = 2\beta_{ax}$, where α is the graze angle on the mirror. The angular ray deviation produced by a local azimuthal slope error of a mirror, β_{az}, is $\gamma_{az} = 2\beta_{az} \sin\alpha$. For $\alpha = 1°$, the sensitivity to axial slope errors is 57× larger than the sensitivity to azimuthal slope errors, so we will ignore the effect of azimuthal slope errors. There are two reflections, and if the axial slope errors are uncorrelated between the two mirrors, then the ray deviation $\gamma_{ax} \approx 2\sqrt{2}\beta_{ax}$. If β_{ax} represents the RMS axial slope error of the mirrors, then the RMS radius of the geometric point-spread function (PSF) is γ_{ax}. Converting a Gaussian distribution of ray positions to a half-power diameter (HPD) requires multiplying by a factor of 1.36, so $HPD \approx 3.85\ \beta_{ax}$. For a desired telescope angular resolution of 0.5 arcsec HPD, with 0.25 arcsec HPD allocated to mirror figure (as was adopted for *Lynx* [14]), $\beta_{ax} \approx 0.065$ arcsec RMS. The measurement uncertainty should contribute only a small portion of this, say $u_{\beta ax} < \beta_{ax}/3 \approx 0.022$ arcsec RMS. If the metrology contributes systematic error, then the measurement uncertainty contribution should be lower by a factor of $\sqrt{2}$, or $u_{\beta ax} < 0.015$ arcsec RMS. In the remainder of this section we shall assume a measurement uncertainty requirement of $u_{\beta ax} < 0.022$ arcsec RMS.

To put an axial slope measurement uncertainty in the context of interferometry, which measures height, we can assume a form of the height error and calculate the relationship between RMS height and RMS slope. If the height error is sinusoidal with spatial wavelength Λ, $z = a \sin(2\pi y/\Lambda)$, then for the length of the mirror equal to an integer multiple of $\Lambda/2$, the RMS height is $w = a/\sqrt{2}$ and the RMS slope is $\beta_{ax} = (2\pi/\Lambda)w$. For a spatial wavelength of $\Lambda = 100\ mm$ and $\beta_{ax} = 0.022$ arcsec RMS, $w = 1.7\ nm\ RMS$.

To summarize, measuring the axial figure error of X-ray mirror segments that would be suitable for a telescope with 0.5 arcsec HPD angular resolution would require axial slope measurement uncertainty around 0.022 arcsec RMS, corresponding to around 1.7 nm RMS height measurement uncertainty. The SUTs have nearly cylindrical shapes, but with a departure that cannot be ignored.

3. EXTRACTING CONE ANGLE AND AXIAL FIGURE

We have previously demonstrated that ASM can accurately extract lines of a SUT and reference along the shifting direction. However, the relationship between the LUTs is undefined: they have unknown tilt and piston (translation along the cylinder radial direction) with respect to one another. Uncertainty in tilt of the LUTs is an uncertainty in the axial slope error, or local cone angle, and significantly affects X-ray imaging performance. Uncertainty in piston between LUTs leads to uncertainty in azimuthal slope error, therefore the piston uncertainty is not required to be at the nanometer level. We will first review the extraction process for shifting the SUT along the axial direction to extract the profile of each LUT, and we will then extend this to extract the slope of each LUT after adding a single shift in the azimuthal direction.

3.1 Extracting the LUT profiles by shifting along the axial direction

Separating the surface height error of a LUT and a reference in one dimension, incorporating the effects of rigid body tilts, has been covered by Elster previously [15], and here we review this process for a single shift (i.e., two measurements). We ignore any edge effects, assuming that the SUT is larger than the reference and we are only interested in extracting the portions of the LUT that are present in both measurements. For comparing the SUT against a cylindrical wavefront produced by the null optics, we are measuring the profile of the SUT in the radial direction of the cylinder, as a function of the y-coordinate, so we denote $r_{LUT}(y)$ as the profile of the LUT.

A measurement is the difference between the profile of the LUT, $r_{LUT}(y)$, and the profile of the corresponding line on the reference (which includes a reference surface plus wavefront error contributed by null optics), $r_{REF}(y)$. For later convenience, we separate the tilt of each line, α_{LUT} and α_{REF}, from the remaining profile. The first measurement is the difference between these two profiles,

$$M_0(y) = r_{LUT}(y) - r_{REF}(y) + \alpha_{LUT} y - \alpha_{REF} y, \tag{1}$$

and the second measurement is the difference between the LUT shifted by a distance Δy and the same reference. A rigid body tilt α and piston β is applied to the LUT,

$$M_1(y) = r_{LUT}(y - \Delta y) - r_{REF}(y) + \alpha_{LUT} \cdot (y - \Delta y) - \alpha_{REF} y + \alpha y + \beta. \tag{2}$$

The difference of the two measurements is,

$$\Delta M(y) = M_1(y) - M_0(y) = r_{LUT}(y - \Delta y) - r_{LUT}(y) - \alpha_{LUT} \Delta y + \alpha y + \beta, \tag{3}$$

which contains only terms from the LUT and not from the reference. If the measurements are discretized into pixels, and the shift distance Δy is an integer number of pixels, then the y-coordinate may be discretized as $y_i = y_0 + i\Delta y$. Rearranging Eq. 3, the profile of the LUT at each point may be calculated as,

$$r_{LUT}(y_i) = r_{LUT}(y_{i-1}) - \Delta M(y_i) - \alpha_{LUT} \Delta y + \alpha y_i + \beta. \tag{4}$$

Recursively applying this equation leads to,

$$r_{LUT}(y_i) = r_{LUT}(y_0) - \alpha_{LUT} \Delta y i + \beta i + \alpha \sum_{j=0}^{i-1} y_{i-j} - \sum_{j=0}^{i-1} \Delta M(y_{i-j}). \tag{5}$$

Substituting $y_{i-j} = y_0 + (i-j)\Delta y$ into the second summation and simplifying, the result is,

$$r_{LUT}(y_i) = r_{LUT}(y_0) + i\left(\alpha y_0 + \frac{1}{2}\alpha\Delta y - \alpha_{LUT}\Delta y + \beta\right) + \alpha\frac{1}{2}i^2\Delta y - \sum_{j=0}^{i-1}\Delta M(y_{i-j}). \tag{6}$$

Here, the first term is a constant, the second term is a tilt, the third term is a quadratic error, and the last term contains all higher-order terms with spatial wavelengths $\Lambda \geq 2\Delta y$ (aliasing occurs at spatial wavelengths below this Nyquist limit). Note that the higher-order terms are independent of α or β. The LUT tilt, α, must be known to measure the quadratic term. For a single LUT, tilt represents a rigid body motion and is generally not of interest. For an X-ray mirror with multiple LUTs, however, the tilt of each LUT, α_{LUT}, represents a local cone angle error. It is therefore desirable to measure this term, which is unknown if β or α_{LUT} are unknown. The next sections detail how both α and α_{LUT} may be extracted.

3.2 Measuring the tilt motion, α

The tilt of each LUT is $\alpha(\theta_y)$ and is a function of the azimuthal coordinate θ_y. In ASM, we measure this tilt using two pre-characterized flat mirrors ("known artifact mirrors", KAMs) to either side of the SUT, at angles $\theta_y = \phi_{KAM1}$ and $\theta_y = \phi_{KAM2}$. Each KAM may be treated as an LUT, but with known $r_{LUT}(y) = r_{KAM1}(y)$ or $r_{LUT}(y) = r_{KAM2}(y)$. Rearranging Eq. 3 for each KAM leads to

$$\begin{aligned}\alpha_{KAM1}y + \beta_{KAM1} &= \Delta M_{KAM1}(y) + r_{KAM1}(y) - r_{KAM1}(y-\Delta y),\\ \alpha_{KAM2}y + \beta_{KAM2} &= \Delta M_{KAM2}(y) + r_{KAM2}(y) - r_{KAM2}(y-\Delta y),\end{aligned} \tag{7}$$

where α_{KAM1} and α_{KAM2} may be calculated by fitting the right-hand sides of Eqs. 7 to a linear function.

As the SUT rotates by pitch angle $e_{\theta x}$ and by a clocking angle $e_{\theta z}$, a line located at azimuth angle θ_y will appear to tilt by

$$\alpha(\theta_y) = e_{\theta x}\cos(\theta_y) + e_{\theta z}\sin(\theta_y). \tag{8}$$

The two rigid body motions of the SUT, $e_{\theta x}$ and $e_{\theta z}$, may be calculated from the measured KAMs tilts α_{KAM1} and α_{KAM2},

$$\begin{aligned}e_{\theta x} &= \frac{\alpha_{KAM1}\sin(\phi_{KAM2}) - \alpha_{KAM2}\sin(\phi_{KAM1})}{\cos(\phi_{KAM1})\sin(\phi_{KAM2}) - \cos(\phi_{KAM2})\sin(\phi_{KAM1})},\\ e_{\theta z} &= \frac{\alpha_{KAM1}\cos(\phi_{KAM2}) - \alpha_{KAM2}\cos(\phi_{KAM1})}{\sin(\phi_{KAM1})\cos(\phi_{KAM2}) - \sin(\phi_{KAM2})\cos(\phi_{KAM1})},\end{aligned} \tag{9}$$

which simplify, for $\phi_{KAM1} = -\phi_{KAM2}$, to

$$e_{\theta x} = \frac{\alpha_{KAM1} + \alpha_{KAM2}}{2\cos(\phi_{KAM})}, \qquad e_{\theta z} = \frac{\alpha_{KAM1} - \alpha_{KAM2}}{2\sin(\phi_{KAM})}. \tag{10}$$

3.3 Measuring the LUT tilt, α_{LUT}

After performing an axial shift, the profile at each azimuth coordinate, θ_y, is known except for their tilts, $\alpha_{LUT}(\theta_y)$. Like axial shifting, we perform a lateral shift by an angle $\Delta\theta_y$ (equal to one pixel), add a tilt $\alpha(\theta_y - \Delta\theta_y)$, and take a second measurement. Recalling Eq. 1 and generalizing to two dimensions, the first measurement is

$$M_0(y,\theta_y) = r_{LUT}(y,\theta_y) - r_{REF}(y,\theta_y) + \alpha_{LUT}(\theta_y)y - \alpha_{REF}(\theta_y)y. \tag{11}$$

The second measurement is,

$$M_1(y,\theta_y - \Delta\theta_y) = r_{LUT}(y,\theta_y - \Delta\theta_y) - r_{REF}(y,\theta_y) + \alpha_{LUT}(\theta_y - \Delta\theta_y)y - \alpha_{REF}(\theta_y)y + \alpha(\theta_y)y + \beta(\theta_y). \tag{12}$$

The difference of the two measurements is,

$$\Delta M(y,\theta_y) = r_{LUT}(y,\theta_y - \Delta\theta_y) - r_{LUT}(y,\theta_y) + \left[\alpha_{LUT}(\theta_y - \Delta\theta_y) - \alpha_{LUT}(\theta_y)\right]y + \alpha(\theta_y)y + \beta(\theta_y). \quad (13)$$

Discretizing the azimuth coordinate as $\theta_{y,i} = \theta_{y0} + i\Delta\theta_y$, we rearrange Eq. 13 to solve for $\alpha_{LUT}(\theta_y)$,

$$\alpha_{LUT}(\theta_{y,i})y = \alpha_{LUT}(\theta_{y,i-1})y + r_{LUT}(y,\theta_{y,i-1}) - r_{LUT}(y,\theta_{y,i}) - \Delta M(y,\theta_{y,i}) + \alpha(\theta_{y,i})y + \beta(\theta_{y,i}). \quad (14)$$

This equation can be recursively applied to arrive at,

$$\left(\alpha_{LUT}(\theta_{y,i}) - \alpha_{LUT}(\theta_{y,0}) - \sum_{j=0}^{i-1}\alpha(\theta_{y,i-j})\right)y - \sum_{j=0}^{i-1}\beta(\theta_{y,i-j}) = r_{LUT}(y,\theta_{y,0}) - r_{LUT}(y,\theta_{y,i}) - \sum_{j=0}^{i-1}\Delta M(y,\theta_{y,i-j}), \quad (15)$$

where all quantities on the right-hand side are known. The bracketed term on the left-hand side is the y-linear portion of the right-hand side. Within the bracketed term, the first term represents the cone angle variation across the SUT, and the second and third terms represent a cone angle offset. Even if the rigid body motion of the SUT were known, the term $\alpha_{LUT}(\theta_{y,0})$ remains unknown. Therefore, with a lateral shift (a small rotation $\Delta\theta_y$) we can measure the cone angle *variation* of the SUT, but not the cone angle.

The ambiguity in the cone angle can be understood by considering that a conical SUT and a conical reference would produce the same result as a cylindrical SUT and cylindrical reference. In both cases, shifting in the axial direction, without having a reliable measurement of $\beta(\theta_y)$, produces no measurable change in the difference of the two surfaces. Therefore, the two cases cannot be distinguished. Likewise, the radius cannot be known from these measurements alone.

4. CONCLUSIONS AND FUTURE WORK

Astronomical X-ray telescope mirrors require accurate surfaces to form sharp images of energetic objects and processes in the universe. In this paper, we described the metrology requirements that would be required for a telescope with 0.5 arcsecond HPD angular resolution based on the *Lynx* error allocation, and we conclude that around 1.7 nm RMS accuracy is required for low spatial frequencies. We presented the mathematical treatment of extracting axial traces on a cylindrical SUT using axial shift mapping, and how the quadratic term is recovered provided two rigid body motions (pitch and clocking) of the SUT are measured. Furthermore, we presented the mathematical treatment of extracting the cone angle variation of the SUT, which is critically important for X-ray optics. We conclude that an azimuthal shift is sufficient to recover cone angle variation, but that the average cone angle remains unknowable from this process. This work extends the utility of axial shift mapping to recover the most relevant parameters of X-ray mirrors. Future work will entail evaluating the impact of real, non-cylindrical X-ray mirrors on the measurement error, and the effect of cone angle uncertainty on the telescope performance.

ACKNOWLEDGEMENTS

Funding: NASA (80NSSC22K1484, 80NSSC20K0907 and 80NSSC24K0366).

REFERENCES

1. J. A. Gaskin, D. A. Swartz, A. A. Vikhlinin, F. Özel, K. E. Gelmis, J. W. Arenberg, S. R. Bandler, M. W. Bautz, M. M. Civitani, A. Dominguez, M. E. Eckart, A. D. Falcone, E. Figueroa-Feliciano, M. D. Freeman, H. M. Günther, K. A. Havey, R. K. Heilmann, K. Kilaru, R. P. Kraft, K. S. McCarley, R. L. McEntaffer, G. Pareschi, W. Purcell, P. B. Reid, M. L. Schattenburg, D. A. Schwartz, E. D. Schwartz, H. D. Tananbaum, G. R. Tremblay, W. W. Zhang, and J. A. Zuhone, "Lynx X-Ray Observatory: an overview," J. Astron. Telesc. Instrum. Syst. **5**, 021001 (2019).
2. *Pathways to Discovery in Astronomy and Astrophysics for the 2020s* (National Academies Press, 2021).
3. C. Reynolds, E. Kara, R. F. Mushotzky, A. Ptak, M. J. Koss, B. J. Williams, S. W. Allen, F. E. Bauer, M. Bautz, A. Bogadhee, K. B. Burdge, N. Cappelluti, B. Cenko, G. Chartas, K.-W. Chan, L. Corrales, T. Daylan, A. D. Falcone, A. Foord, C. E. Grant, M. Habouzit, D. Haggard, S. Herrmann, E. Hodges-Kluck, O. Kargaltsev, G. W. King, M. Kounkel, L. A. Lopez, S. Marchesi, M. McDonald, E. Meyer, E. D. Miller, M. Nynka, T. Okajima, F. Pacucci, H. R. Russell, S. Safi-Harb, K. G. Strassun, A. Trindade Falcão, S. A. Walker, J. Wilms, M. Yukita, and W. Zhang, "Overview of the advanced x-ray imaging satellite (AXIS)," in *Proc. SPIE* (2023), Vol. 12678, p. 126781E.
4. K. K. Madsen, J. A. García, D. Stern, R. Amini, S. Basso, D. Coutinho, B. W. Grefenstette, S. Kenyon, A. Moretti, P. Morrissey, K. Nandra, G. Pareschi, P. Predehl, A. Rau, D. Spiga, J. Wilms, and W. W. Zhang, "The high energy X-ray probe (HEX-P): instrument and mission profile," Front. Astron. Space Sci. **11**, 1357834 (2024).
5. G. H. Sanders, "The Thirty Meter Telescope (TMT): An International Observatory," J. Astrophys. Astron. **34**, 81–86 (2013).
6. P. Padovani and M. Cirasuolo, "The Extremely Large Telescope," Contemp. Phys. **64**, 47–64 (2023).
7. J. L. Fanson, R. Bernstein, D. Ashby, B. C. Bigelow, G. Brossus, W. S. Burgett, R. T. Demers, B. M. Fischer, F. Figueroa, F. Groark, R. Laskin, R. Millan-Gabet, S. Park, M. Pi, R. Turner, and B. Walls, "Overview and status of the Giant Magellan Telescope project," in *Proc. SPIE* (2022), Vol. 12182, p. 121821C.
8. H. J. Wisniewski, R. K. Heilmann, M. L. Schattenburg, and B. D. Chalifoux, "Axial shift mapping: a self-referencing test for measuring the axial figure of near-cylindrical surfaces," Appl. Opt. **62**, 9307–9316 (2023).
9. L. P. VanSpeybroeck and R. C. Chase, "Design Parameters of Paraboloid-Hyperboloid Telescopes for X-ray Astronomy," Appl. Opt. **11**, 440–445 (1972).
10. R. C. Chase and L. P. VanSpeybroeck, "Wolter-Schwarzschild Telescopes for X-Ray Astronomy," Appl. Opt. **12**, 1042–1044 (1973).
11. W. W. Zhang, K. D. Allgood, M. Biskach, K.-W. Chan, M. Hlinka, J. D. Kearney, J. R. Mazzarella, R. S. McClelland, A. Numata, R. E. Riveros, T. T. Saha, and P. M. Solly, "High-resolution, lightweight, and low-cost x-ray optics for the Lynx observatory," J. Astron. Telesc. Instrum. Syst. **5**, 021012 (2019).
12. C. T. DeRoo, R. Allured, V. Cotroneo, E. N. Hertz, V. Marquez, P. B. Reid, E. D. Schwartz, A. A. Vikhlinin, S. Trolier-McKinstry, J. Walker, T. N. Jackson, T. Liu, and M. Tendulkar, "Deterministic figure correction of piezoelectrically adjustable slumped glass optics," J. Astron. Telesc. Instrum. Syst. **4**, 019004 (2018).
13. K. Kilaru, B. D. Ramsey, W. H. Baumgartner, S. D. Bongiorno, D. M. Broadway, P. R. Champey, J. M. Davis, S. L. O'Dell, R. F. Elsner, J. A. Gaskin, S. Johnson, J. K. Kolodziejczak, O. J. Roberts, D. A. Swartz, and M. C. Weisskopf, "Full-shell x-ray optics development at NASA Marshall Space Flight Center," J. Astron. Telesc. Instrum. Syst. **5**, 1 (2019).
14. A. A. Vikhlinin, F. Özel, and J. A. Gaskin, *Lynx X-Ray Observatory Concept Study Report* (The Lynx Team, 2020).
15. C. Elster, I. Weingärtner, and M. Schulz, "Coupled distance sensor systems for high-accuracy topography measurement: Accounting for scanning stage and systematic sensor errors," Precis. Eng. **30**, 32–38 (2006).